Eu²⁺ Site Preferences in the Mixed Cation K₂BaCa(PO₄)₂ and Thermally Stable Luminescence

Jianwei Qiao[†], Lixin Ning[#,*], Maxim S. Molokeev[‡,Δ,⊥], Yu-Chun Chuang[§], Quanlin Liu[†], Zhiguo Xia[†,*]

[†]The Beijing Municipal Key Laboratory of New Energy Materials and Technologies, School of Materials Sciences and Engineering, University of Science and Technology Beijing, Beijing 100083, China

[#]Anhui Key Laboratory of Optoelectric Materials Science and Technology, Department of Physics, Anhui Normal University, Wuhu, Anhui 241000, China

[‡]Laboratory of Crystal Physics, Kirensky Institute of Physics, Federal Research Center KSC SB RAS, Krasnoyarsk 660036, Russia

[Δ]Siberian Federal University, Krasnoyarsk, 660041, Russia

[⊥]Department of Physics, Far Eastern State Transport University, Khabarovsk, 680021 Russia

[§] National Synchrotron Radiation Research Center, Hsinchu 300, Taiwan

ABSTRACT: Site preferences of dopant Eu²⁺ on the locations of K⁺, Ba²⁺ and Ca²⁺ in mixed cations K₂BaCa(PO₄)₂ (KBCP) are quantitatively analyzed via a combined experimental and theoretical method to develop a blue-emitting phosphor with thermally stable luminescence. Eu²⁺ ions are located at K2 (M2) and K3 (M3) sites of KBCP, with the latter occupation relatively more stable than the former, corresponding to emissions at 448 and 478 nm, respectively. KBCP:Eu²⁺ phosphor exhibits highly thermal stable luminescence even up to 200 °C, which is interpreted as due to a balance between thermal ionization and recombination of Eu²⁺ 5d excited-state centers with the involvement of electrons trapped at crystal defect levels. Our results can initiate more exploration of activator site engineering in phosphors and therefore allows predictive control of photoluminescence tuning and thermally stable luminescence for emerging application in white LEDs.

INTRODUCTION

Phosphor-converted white light-emitting diodes (pc-WLEDs) have been extensively considered as the most promising new generation solid state lighting sources due to their environmental friendliness, robustness, and long lifetimes.[1-4] Most commercially available pc-LEDs are based on Y₃Al₅O₁₂:Ce³⁺ (YAG:Ce³⁺) phosphors pumped by blue LEDs, which, however, suffer from poor color-rendering index (R_a < 75) and high correlated color temperatures (CCT > 4500 K) due to the lack of red components.[5] Near ultraviolet (NUV) LEDs assembled with blue, green and red emitting phosphors have been exploited for their high quality white light emission with high color rendering property and superior color uniformity.[6, 7] Nevertheless, thermal quenching (TQ) properties of phosphors seriously affects luminance efficiency and restricts their applications in pc-WLEDs, especially in high power conditions or laser LEDs.[8-10] Therefore, laboratory discovery of phosphors with high luminance and thermal stability is still an imperative challenge.

In terms of the currently used and available phosphors for pc-WLEDs, the number of blue emitting compounds is rather limited. Although the commercial blue emitting

BaMgAl₁₀O₁₇:Eu²⁺ and Sr₃MgSi₂O₈:Eu²⁺ phosphors show a high luminance efficiency at room temperature, the TQ effect seriously reduce the emission intensity during the operation of LED.[11] Various techniques have been employed to minimize TQ, such as by using high structural rigidity phosphor, ceramic coating (SiO₂, TiO₂) over phosphors, and glass-ceramic phosphors.[11-17] In particular, it has been recently demonstrated that crystal defects may play a positive role in diminishing TQ of Eu²⁺ luminescence through an energy transfer process from defect levels to the Eu²⁺ 5d levels owing to the inequivalent substitution of Eu²⁺ in Na⁺ site in Na₃Sc₂(PO₄)₃ phase.[18] It is believed that mixed cations in the host could initiate the versatile site occupations of activators, and thus the discovery of new phosphor systems is beneficial for optimization of the luminescence properties toward practical applications.

In recent years, our group has proposed a useful methodology for the discovery of new LED phosphors by mineral-inspired prototype evolution and new phase construction, which have been effectively applied to the discovery of new phosphors.[19-21] In addition, ABPO₄:Eu²⁺ phosphors (A = Li, Na, K, Ru, B=Ca, Sr, Ba) with β-K₂SO₄

type structure have been widely investigated due to their high thermal stability, such as $KSrPO_4:Eu^{2+}$, $KBaPO_4:Eu^{2+}$ and $RbBaPO_4:Eu^{2+}$.[22-24] Enlightened by the above reports, in the present work we successfully designed a novel blue-emitting phosphor $K_2BaCa(PO_4)_2:Eu^{2+}$ (KBCP:Eu^{2+}) from the β-K_2SO_4-type structure, which exhibits high luminescence thermal stability. Structural evolution, photoluminescence properties, and temperature-dependent behaviors were discussed in detail. Optimization of Eu^{2+} concentration revealed that the luminescence intensity of KBCP:3%Eu^{2+} exhibits zero thermal quenching up to 200 °C. This behavior was explained as due to a balance between thermal ionization and recombination of Eu^{2+} 5d excited-state centers, involving the electrons trapped at crystal defect levels. This study may open up a new understanding and perspective for designing high thermal stability phosphors.

EXPERIMENTAL SECTION

Synthesis. A series of KBCP:Eu^{2+} (x = 0.5–9%) were synthesized by the high temperature solid-state method. The stoichiometric mixtures of K_2CO_3 (A.R.), $BaCO_3$ (A.R.), $CaCO_3$(A.R.), $NH_4H_2PO_4$ (A.R.), and Eu_2O_3 (99.99%) were ground in an agate mortar and filled into an alumina crucible. Mixtures were sintered under a reducing atmosphere (5% H_2 /95% N_2) at 1200 °C for 4 h and then quenched to room temperature, and finely ground with a mortar for further characterization.

Characterization: Powder X-ray diffraction (XRD) measurements were performed on a D8 Advance diffractometer (Bruker Corporation, Germany) at 40 kV and 40 mA with Cu Ka radiation (λ=1.5406 Å). Synchrotron X-ray
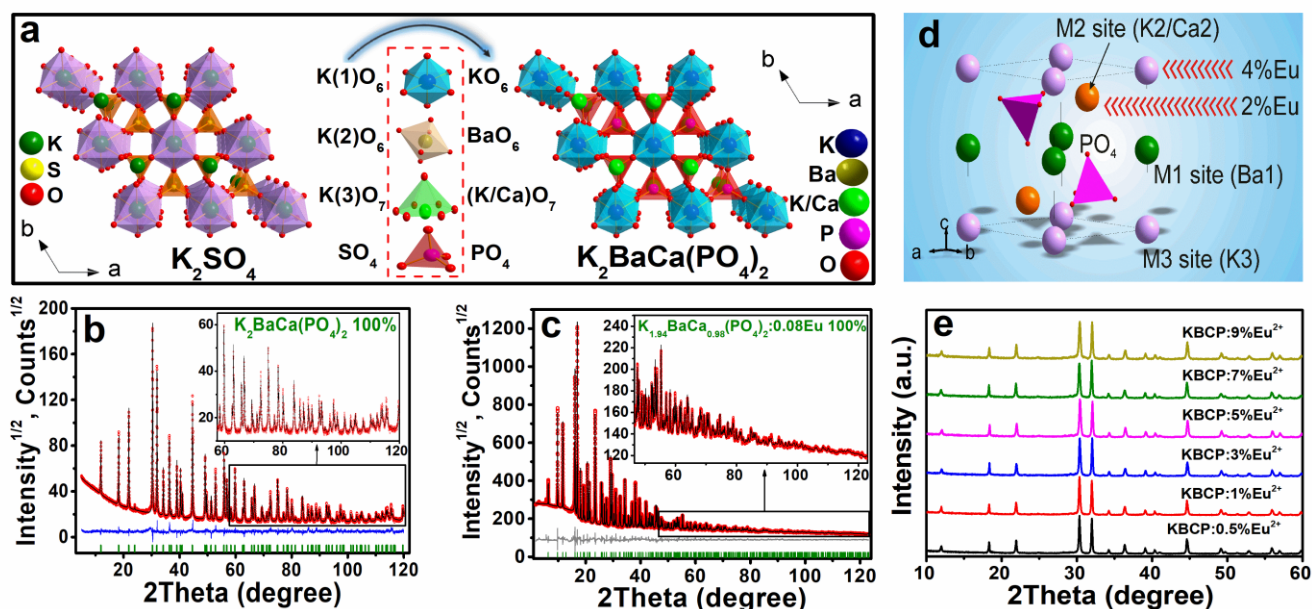
Figure 1. (a) Structural phase transformation model from β-K_2SO_4 prototype to new phase of KBCP via the different substitution construction on different K sites. (b) XRD and (c) SXRD profile for Rietveld refinement result of KBCP and KBCP:9%Eu^{2+}, respectively. (d) Crystal structure of KBCP:9%Eu^{2+} and the occupied rates of Eu^{2+}. (e) XRD patterns of as-prepared KBCP:xEu^{2+} (x = 0.5–9%).

diffraction (XRD) measurements were performed on a D8 Advance diffractometer (Bruker Corporation, Germany) at 40 kV and 40 mA with Cu Ka radiation (λ=1.5406 Å). Synchrotron X-ray powder diffraction (SXRD) data were collected at TPS 09A (Taiwan Photon Source) of the National Synchrotron Radiation Research Center with a calibrated wavelength of 0.82656 Å. Rietveld structure refinements were conducted using TOPAS 4.2.[25] The morphology and microstructure of the samples were investigated using a scanning electron microscope (SEM, JEOL JSM-6510A). The photographs of microcrystal particle were obtained by a Nikon LV100ND optical microscope. The photoluminescence (PL), photoluminescence excitation (PLE) spectra and temperature dependent luminescence spectra were detected by a Hitachi F-4600 fluores-

cence spectrophotometer. The decay curve was collected by FLSP920 fluorescence spectrophotometer equipped with an nF900 flash lamp as the excitation source. The electroluminescence spectra, color-rendering index (Ra), and color temperature (CCT) of the as-fabricated w-LEDs were measured using a UV-Vis-near IR spectrophotocolorimeter (PMS-80, Everfine).

COMPUTATIONAL METHODOLOGY

The KBCP:Eu^{2+} crystals were modeled by 2 × 2 × 2 supercells containing 112 atoms, in which one of the $Ba^{2+}/K^+/Ca^{2+}$ ions was substituted by a Eu^{2+}. The nearest distance between Eu^{2+} ions in the periodic supercell systems is larger than 10.0 Å, which is large enough to avoid their mutual influence in view of the localized 4f electron-

ic states of Eu²⁺. Periodic DFT calculations were performed using the PBE+U approach with $U = 2.5$ eV for the Eu 4f electrons,[26, 27] as implemented in the VASP code.[28, 29] The Ba($5s^2 5p^6 6s^2$), Ca($3p^6 4s^2$), K($3p^6 4s^1$), P($3s^2 3p^3$), O($2s^2 2p^4$), and Eu($5s^2 5p^6 4f^7 6s^2$) were treated as valence electrons, and their interactions with the cores were described by the projected augmented wave (PAW) approach.[30] The atomic structures of the supercells were fully optimized until the total energies and the forces on the atoms were converged to 10^{-6} eV and 0.01 eV Å⁻¹. For the calculation of thermodynamic charge transition levels of crystal defects, the PBE0 hybrid functional was employed,[31] as this functional has been shown to improve the results of the band gaps and defect properties in oxides when compared with pure PBE functional.[32] One k-point Γ was used to sample the Brillouin zone, and the cutoff energy of the plane-wave basis was set to 530 eV.

RESULTS AND DISCUSSION

Crystal Structure and Morphology

In β-K₂SO₄ type structures, there are three independent K cation sites (K(1), K(2) and K(3)), which provides a generic platform to design new β-K₂SO₄ type compounds. As a representative, phosphates with the general formula ABPO₄ have been synthesized by the cosubstitution of K⁺→A⁺ (A = Li, Na, Rb, Cs), K⁺→B²⁺ (B = Ca, Sr, Ba, Mg, Zn), and SO₄→PO₄. Here, we successfully designed and synthesized a new ABPO₄ type phosphate

K₂BaCa(PO₄)₂ through co-substitution of K(1)O₆→KO₆, K(2)O₆ → BaO₆, K(3)O₇ → (K/Ca)O₇ and SO₄ → PO₄, as shown in Figure 1a. To characterize the structure of the material, Rietveld refinement of the powder XRD data was conducted (Figure 1b). Almost all peaks in the XRD pattern can be indexed by trigonal cell (P-3m1) with parameters close to those for NaBaPO₄.[33] Therefore, NaBaPO₄ crystal structure was used as the starting model for Rietveld refinement. There are two Ba sites (M1 and M2 sites) in the NaBaPO₄ structure, with the M1 sites being fully occupied by Ba²⁺ ion and the M2 sites being occupied by 50% Ba²⁺ and 50% Na⁺ ions. Additionally, NaBaPO₄ has one fully occupied Na site (M3 site). Our refinement showed that the M1 site in K₂BaCa(PO₄)₂ should be occupied by very heavy ion, but not for the M2 site. Thus, we suggest that, in K₂BaCa(PO₄)₂, Ba²⁺ and K⁺ ions fully occupy the M1 and M3 sites, respectively, with the M2 sites being occupied by Ca²⁺ and K⁺ ions. As for the Ca/K ratio at the M2 site, preliminary refinement showed that the M1 sites were fully occupied by Ba²⁺ ions without any traces of Ca²⁺ or K⁺, and consequently the M2 sites should be occupied by 50% Ca²⁺ and 50% K⁺ ions in accordance to the chemical formula K₂BaCa(PO₄)₂ (Figure S1). Final refinement of this model was stable and gives low R-factors (Table S1, Figure 1b). Coordinates of atoms and main bond lengths are given in Table S2 and Table S3, respectively. The crystallographic information file (CIF) of this new phase K₂BaCa(PO₄)₂ is also presented in the Supporting Information.
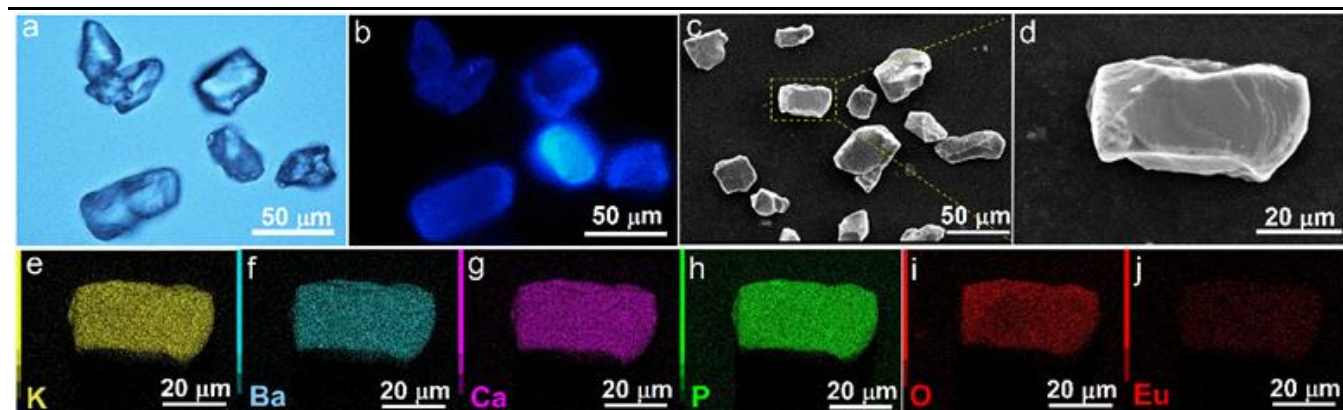
Figure 2. (a) Optical microscope photographs of the KBCP: 3%Eu²⁺ microcrystal particles without (a) and with 365 nm UV excitation (b). SEM images of the KBCP:Eu²⁺ microcrystal particles (c) and the enlarged one particle (d). EDS elemental mapping of the cross section of KBCP:3%Eu²⁺ (e-j).

To further determine which sites were occupied by Eu ions, Rietveld refinement of high-quality synchrotron XRD data was conducted. There are three different sites which can be potentially occupied by Eu ions: Ba (M1), Ca2/K2 (M2), and K3 (M3) sites (Figure S1). Eu occupations in all these sites were refined by taking into account that the sum of all occupancies in each site is equal to 1. The refinement was stable and gives low R-factors (Table S1, Figure 1d). Coordinates of atoms and main bond lengths are in Table S2 and Table S3 respectively. Chemical formula from refinement was K₁.₉₄₀₍₂₎BaCa₀.₉₈₀₍₂₎(PO₄)₂:0.080(2)Eu and the obtained Eu

doping level (8.0(2)%) is close to the suggested one (9%). Analysis of Eu distribution over the host sites revealed that only M2 and M3 sites are occupied by Eu (Table S2), and the amount of Eu ions at the latter sites is two times larger than that at the former sites (Figure 1d). The XRD patterns of as-obtained KBCP:xEu²⁺ (1% ≤ x ≤ 9%) are depicted in Figure 1e. No diffraction peaks of any other phases are detected even when x = 9%, indicating that all samples are of pure phase with the trigonal (P-3m1) structure.

To characterize the morphology of KBCP:Eu²⁺ phosphors, optical microscope photographs, SEM, and EDS

mapping were carried out. The optical microscope photographs of KBCP:Eu²⁺ particles without and with 365 nm UV light excitation are shown in Figure 2a and Figure 2b, respectively. The bright blue light (Figure 2b) from the KBCP:Eu²⁺ microcrystals indicates that KBCP:Eu²⁺ phosphor may possess a high luminous efficiency. Figure 2c and Figure 2d depict the SEM images of KBCP:Eu²⁺ microcrystals at different scales, and the smooth surfaces demonstrate that the microcrystals have a high degree of crystallinity. The elemental mapping images (Figure 2e-j) evidence that K, Ba, Ca, P, O, and Eu are very homogeneously dispersed within the phosphor particles. Moreover, both the optical microscopy and SEM images show that the particle morphology and the sizes of the as-prepared samples is very similar in the micrometer range, which benefits the fabrication for white LEDs devices.

Eu²⁺ Site Occupations by DFT

Eu²⁺ site occupations in mixed cations $K_2BaCa(PO_4)_2$ were also investigated by using DFT calculations. To do this, however, the occupation disorder of Ca/K at the M2 site of the host needs to be properly modeled first. This was achieved by considering all possible configurations of Ca and K over the 16 M2 sites of a 2 × 2 × 2 supercell of $K_2BaCa(PO_4)_2$. With the occupancy ratio fixed at Ca/K = 1, there are in principle (16)!/(8!×8!) = 12870 different configurations, which is extensive enough to explore any short-range order in their distribution. When the crystal symmetry of the supercell was taken into account with the method reported in reference 34,[34] the number of crystallographically distinct configurations necessary for calculations reduced to 204. Their relative occurrence probabilities P_m (m = 1, ..., 204) with multiplicities Ω_m were then evaluated by $P_m = \frac{1}{Z} \Omega_m \exp\left(-\frac{E_m}{kT}\right)$, where E_m is the DFT total energy, k is the Boltzmann constant, T (= 1473 K) is the synthesis temperature of the materials, and Z is the partition function. P_m comprises both the energetic and the multiplicity information, and can thus be used for direct comparison of independent configurations. DFT calculations revealed that that there are six inequivalent configurations constituting the major part of the total ensemble, with the occurrence probabilities P = 0.194, 0.134, 0.132, 0.092, 0.077, and 0.065, respectively. The probabilities for the other inequivalent configurations are each lower than 0.030. The undoped supercells with these six configurations were then employed to investigate Eu²⁺ site occupations at the host cationic sites.

The relative occupancies of Eu at the K2 (M2) and K3 (M3) sites were first evaluated. In each of the above six undoped supercells, an Eu atom was substituted successively for the 16 K atoms (including eight K2 atoms and eight K3 atoms). From the calculated DFT total energies, the occurrence probability P_i of an Eu occupying a K2 or K3 site was calculated, by using $P_i = \frac{1}{Z_{tot}} \exp\left(-\frac{E_i}{kT}\right)$, ($i$ = 1, ..., 96), where E_i is the DFT total energy and Z_{tot} is the partition function. By summing the values of P_i for Eu at the K2 and K3 sites, respectively, it was found the dopant

Eu prefers to be at the K3 site over the K2 site, with the relative overall probabilities being 0.626 and 0.374, respectively. This is consistent with the Rietveld refinement result that the occupancy of Eu at the K3 site is approximately two times larger than that at the K2 site.

Next, to investigate site preferences of Eu at the Ba1 (M1) and Ca2 (M2) sites relative to those at the K2 (M2) and K3 (M3) sites, the 2 × 2 × 2 undoped supercell with the most stable Ca2/K2 configuration (P = 0.194) was chosen for this investigation. The defect formation energies (E_f) were calculated for Eu_{Ba1}, Eu_{Ca2}, nearest-neighbor (NN) Eu_{K2}–(V_{K3}, K_{Ba}, or K_{Ca}), and NN Eu_{K3}–(V_{K2}, K_{Ba}, or K_{Ca}) substitutions. Detailed calculation procedure and results are given in the SI (Supporting information). The results show that Eu occupations at the Ba1 and Ca2 sites are energetically very unfavorable (by > 2.5 eV in E_f) compared to the occupations at the K2 and K3 sites. It is thus expected that Eu²⁺ ions are mostly located at the K2 and K3 sites, consistent with experimental results. Additionally, it shows that for a given Eu_{K2} or Eu_{K2} substitution, the charge compensation by a NN V_K is much more stable than those by a NN K_{Ca} or K_{Ba}. It is worth noting that, although only one representative undoped supercell was employed to calculate the defect formation energies, the much higher E_f values of Eu_{Ba1} and Eu_{Ca2} than those of Eu_{K2} and Eu_{K3} ensures that the conclusion would not change if other undoped supercells were included for the investigation. Therefore, DFT calculations predict that most Eu²⁺ ions are located at K2 (M2) and K3 (M3) sites of KBCP, with the latter occupation relatively more stable than the former, supporting the results from Rietveld refinements.
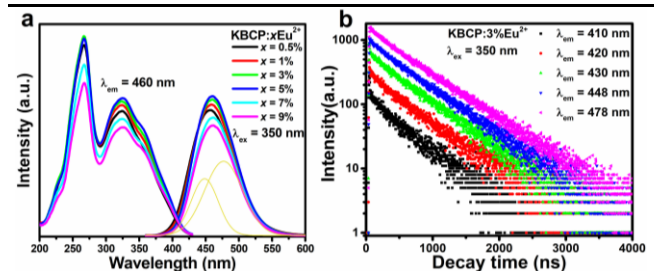
Figure 3. (a) PLE and PL spectra of KBCP:xEu²⁺ phosphors (x = 0.5–9%). (b) Decay curves of KBCP:3%Eu²⁺ emissions at wavelengths from 410 to 448 nm under 350 nm excitation at room temperature.

Photoluminescence Properties

To evaluate photoluminescence properties of KBCP:Eu²⁺, the PLE and PL spectra of the samples with different Eu²⁺ concentrations are measured and shown in Figure 3a. Under 350 nm UV excitation, the optimum emission was exhibited by the KBCP:3%Eu²⁺ sample. All the samples show a typical broad band emission corresponding to the 5d→4f transition of Eu²⁺, with the maximum emission wavelength at 460 nm. The broad emission band can be well decomposed into two Gaussian curves (dark yellow dashed line) with maxima at 448 and 478 nm, indicating

the presence of two different Eu²⁺ luminescence centers, in agreement with the above results of Eu²⁺ site occupation from Rietveld refinements and DFT calculations. The emission with the higher (lower) intensity and maximum at 478 nm (448 nm) can be ascribed to Eu²⁺ at K3 (K2) sites, in view of the larger occupancy and smaller coordination polyhedron of Eu at the K3 site than those at the K2 site. Figure 3a also shows the PLE spectra of KBCP:xEu²⁺ at room temperature, which display a typical two-band structure with band maxima at 265 and 327 nm, as a result of superposition of contributions from Eu²⁺ at the K2 and K3 sites.

The decay behaviors of Eu²⁺ emissions at wavelengths from 410 to 478 nm for KBCP:3%Eu²⁺ were measured and shown in Figure 3b. All the decay curves can be well fitted by a double-exponential function expressed as,

$$I = A_1 \exp\left(-\frac{t}{\tau_1}\right) + A_2 \exp\left(-\frac{t}{\tau_2}\right) \tag{1}$$

where I is the luminescence intensity, τ_1 and τ_2 are the fast and slow components of the decay time, and A_1 and A_2 are the corresponding fitting parameters. The fitting results are present in Table S4. It shows that each decay curve is dominated by the slow component, with the decay time in the range of 528–617 ns. The fast and slow components can be ascribed to Eu²⁺ located at K2 and K3 sites, respectively, in view of their relative occupancies by Eu²⁺. The average lifetime gradually becomes longer with the increase of the monitored wavelength, as a result of the increasing contribution of the slow component corresponding to the emission of Eu²⁺ at K3 sites.

Zero-thermal quenching in KBCP:Eu²⁺ phosphor

As one of critical factor to evaluate the potential of a new phosphor used for LEDs, the thermal quenching behaviors of the representative KBCP:x%Eu²⁺ (x = 1%, 3%, 5%) samples were measured. Figure 4a illustrates the temperature-dependent emission spectra of KBCP:3%Eu²⁺ from 25 to 300 °C. Under 350 nm excitation, a slight blue-shift of the emission was observed with the increase of temperature. Similar observations were made for KBCP:xEu²⁺ with x=1% and 5% (Figure S2). This could be due to the different sensitivities to temperature of Eu²⁺ emission at the K2 and K3 sites, i.e., the emission intensity of Eu²⁺ at K3 sites decreases slightly faster than that at K2 sites with increasing temperature.

Figure 4b, c shows respectively the temperature dependences of the peak and integrated intensities of Eu²⁺ emissions in KBCP:xEu²⁺ (x = 1 %, 3% and 5%) under 350 nm excitation. From Figure 4b, one sees that the peak intensities of all samples decrease linearly with increasing temperature, among which the peak intensity of KBCP:3%Eu²⁺ at 200 °C remains 96% of the intensity at 25 °C. By contrast, the integrated intensity of KBCP:xEu²⁺ decreases more slowly with the increase of temperature (Figure 4c), and the intensities of all samples at 200 °C remain >95% of that at 25 °C. The different temperature-dependent behaviors of the peak and integrated emission intensities may be attributed to the emission band broad-

ening with increasing temperature. In particular, the KBCP:3%Eu²⁺ sample exhibits a zero thermal quenching up to a temperature of 275 °C. For comparison, the temperature dependence of the emission intensity of commercial LED phosphor YAG:Ce³⁺ were also collected under 455 nm excitation. As shown in Figure 4d, YAG:Ce³⁺ shows about 7% emission loss at 200 °C of the room temperature value, whereas KBCP:3%Eu²⁺ phosphor exhibits zero emission loss. When temperature increases from 25°C to 300 °C, a minimal blue shift (Figure 4i) and red shift (Figure 4ii) are observed for KBCP:Eu²⁺ and YAG:Ce³⁺, respectively. The remarkable thermal quenching behavior indicates that KBCP:Eu²⁺ is desirable for WLED applications.
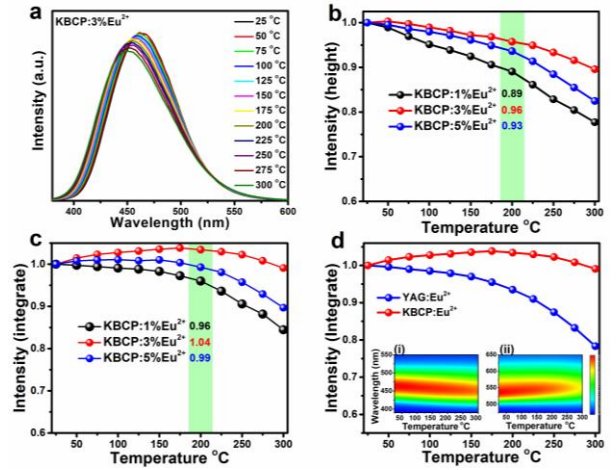
Figure 4. (a) Emission spectra of the KBCP:3%Eu²⁺ sample in the temperature range from 25 to 300 °C. Temperature-dependent normalized emission spectra of KBCP:xEu²⁺ (x= 1%, 3%, 5%) in terms of emission height (b) and area (c) excited at 350 nm. (d) Temperature-dependent normalized emission spectra of KBCP:3%Eu²⁺ in comparison with those of the commercial YAG:Ce³⁺ phosphor.

Mechanism of zero-thermal quenching

The temperature dependence of the integrated emission intensity of Eu²⁺-activated phosphors is usually described by the empirical Arrhenius equation,[35] which implies that the intensity decreases with increasing T, and thus cannot explain the initial rise phase in the thermal quenching behavior of KBCP:3%Eu²⁺ (Figure 4c,d). Recent studies showed that the zero-thermal quenching could be associated with the interaction between Eu²⁺ and crystal defects which act as electron-trapping centers.[18] As such, we performed TL measurements of KBCP:3%Eu²⁺, and the result is displayed in Figure 5a. It shows a broad TL glow curve in the range from 30 to 200 °C, indicating a continuous distribution of trap depths. By fitting the TL curve with two Gaussian bands peaking at 66 and 105 °C, the characteristic trap depths (E_T) were estimated to be 0.68 and 0.76 eV by using the crude relationship $E_T = T/500$ eV, where the temperature T is in units of kelvin (K).[36]

The crystal defects associated with the trap depths could be either potassium vacancies (V_K) which act as the maincharge compensators for the excess charge of Eu_K substitutions, or oxygen vacancies (V_O) which are present due to the reducing conditions during preparation of the materials. To clarify the nature of the defects that could be involved in the zero-thermal quenching, thermodynamic charge transition levels of V_{K2}, V_{K3}, V_{O1}, and V_{O2} were calculated by using hybrid DFT with PBE0 functional. The charge transition level indicates the Fermi level at which the formation energies of a defect in two charge states are equal.[37] The undoped KBCP supercell with the most stable Ca2/K2 configuration was chosen for this investigation. The results are listed in Table S5, and are also schematically depicted in Figure 5b. It shows that $V_{O1,2}$ ($V_{K2,3}$) can behave as trapping centers of electrons (holes) from the conduction (valence) band. In particular, the $\varepsilon(0/-)$ levels of V_{O1} and V_{O2}, which are related to trapping of an electron by a neutral V_O and changing its charge state to -1, are predicted to be 0.42 and 0.82 eV below the bottom of the conduction band. These values are closed to the characteristic trap depths (0.68 and 0.76 eV) as estimated from TL measurements. Therefore, we suppose that the defects involved in the initial rise phase of zero thermal quenching are most likely due to oxygen vacancies in the host material.

Since the net charges of Eu_K and V_O are of the same sign, the two single defects are expected to be far from each other for electrostatic reasons, and thus the conduction band states should be involved in the electron transport between them if it happens. With this in mind, the initial rise of integrated intensity with increasing temperature as observed in the thermal quenching behavior of KBCP:3%Eu²⁺ may be explained by a simplified model as schematically shown in Figure 5c. For the steady state luminescence at a given temperature, there is a balance between thermal ionization of Eu²⁺ 5d electrons into the host conduction band followed by trapping of electrons at defect levels [processes (3) and (4)] and detrapping of electrons at defect levels followed by recombination with Eu³⁺ to yield excited Eu²⁺ 5d centers [processes (5) and (6)]. By using rate equations to model the processes, the following simple expression for the dependence of the emission intensity (I) on temperature (T) can be derived (see the SI for details):

$$I(T) = \frac{I_0}{1+\exp(\Delta E_1/kT)}$$
(2)

where I_0 is a parameter representing the emission intensity at $T = \infty$ K, and $\Delta E_1 = E_{trap} - E_{5d}$ where and E_{trap} (E_{5d}) is the energy separation between the defect level (Eu²⁺ 5d level) and the bottom of the conduction band. If E_{trap} is larger than E_{5d}, then the above expression implies that $I(T)$ increases with increasing T. A good fitting of the expression to the thermal quenching behavior of KBCP:3%Eu²⁺ in the range of $T= 298$–448 K is exhibited in Figure 5d. Thus, the initial rise of the emission intensity with increasing T is most likely due to the fact that an increase of thermal energy is beneficial for

recombination process in comparison with the trapping process. With further increase of temperature, other non-radiative decay processes become increasingly important (e.g., through cross-over between the 4f ground and 5d excited levels or other channels to return to the 4f ground state), and start dominating the temperature-dependent behavior of the emission intensity. Hence the intensity starts to drop with increasing temperature, which may be described by the conventional Arrhenius equation (Figure 5d):

$$I(T) = \frac{I_0}{1+A\exp(-\Delta E/kT)}$$
(3)

where I_0 and I_T is the initial emission intensities of the phosphor at $T = 0$ K and experimental temperature, respectively, A is a constant, ΔE is the activation energy, and k is the Boltzmann constant. The calculated ΔE is 0.51 eV, which is quite high to ensure a small emission loss with the increase of temperature.[38] It is important to realize that in the above simplified model to explain the initial rise phase of thermal quenching behavior of KBCP:3%Eu²⁺, the larger value of trap depth (E_{trap}) than that of the energy separation (E_{5d}) between the Eu²⁺ 5d level and the bottom of the conduction band is a crucial condition. For KBCP:1%Eu²⁺ and KBCP:5%Eu²⁺, this might not be the case, or other non-radiative decay processes are dominant already in the initial phase, as manifested by the thermal quenching behaviors of the samples.
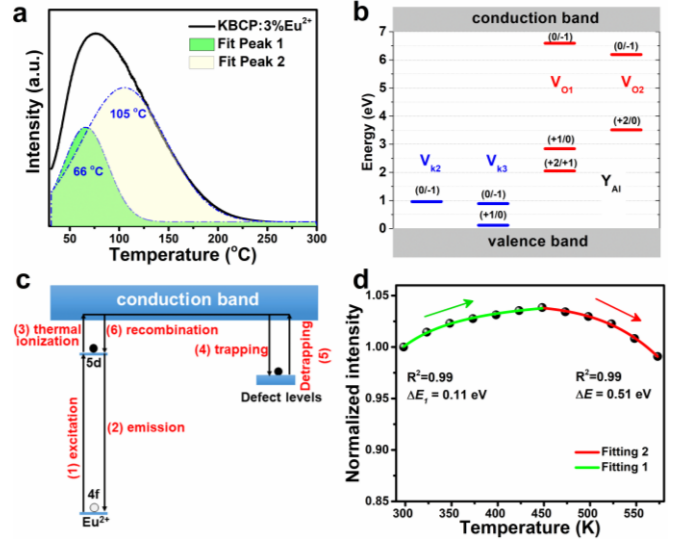

Figure 5. (a) TL curve of KBCP:3%Eu²⁺. (b) Schematic representation of calculated thermodynamic charge transition levels for $V_{K2,3}$ and $V_{O1,2}$ in KBCP by using the DFT-PBE0 method. (c) A simplified model to describe the initial rise of the integrated emission intensity with increasing temperature in KBCP:3%Eu²⁺. (d) Nonlinearity fitting of the thermal quenching behavior of KBCP:3%Eu²⁺ by two different equations.

CIE chromaticity coordinates and application for WLEDs

The CIE chromaticity coordinates of KBCP:3%Eu²⁺ phosphor are shown in Figure 6a. KBCP:Eu²⁺ appears as homo-

geneous powder and shows bright blue light with the CIE coordinate of (0.142, 0.116). In addition, the internal quantum efficiency KBCP:3%Eu^{2+} is 83% at room temperature. Finally, pc-WLED was fabricated by combining a 365 nm near-UV LED chip with the mixture of blue (KBCP:Eu^{2+}), commercial green (Ba$_2$SiO$_4$:Eu^{2+}) and red (CaAlSiN$_3$:Eu^{2+}) phosphors, as presented in Figure 6b. The CCT, Ra value and the CIE coordinate of the as obtained WLED is 5326 K, 85 and (0.328, 0.338), respectively. These results demonstrated that KBCP:Eu^{2+} has potential to serve as blue-emitting phosphor for pc-LED.
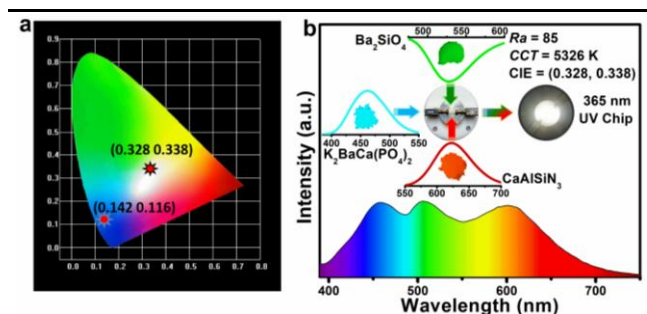
Figure 6. (a) CIE color coordinates of KBCP:3%Eu^{2+} and the fabricated WLED. (b) Photograph and electroluminescent spectrum of WLED fabricated by blue (KBCP:Eu^{2+}), green (Ba$_2$SiO$_4$:Eu^{2+}) and red (CaAlSiN$_3$:Eu^{2+}) phosphors driven by a UV chip (λ_{max} = 365 nm).

CONCLUSION

In summary, we have successfully developed a new blue-emitting KBCP:Eu^{2+} phosphor from the β-K$_2$SO$_4$ type host with thermally stable luminescence. The refinement analysis from XRD results and DFT calculation support that Eu^{2+} occupied the K2 (M2) and K3 (M3) cationic sites of KBCP. It was proposed that the competition between thermal ionization and recombination of Eu^{2+} 5d excited-state centers lead to the high thermal stability of KBCP:Eu^{2+}. The fabricated WLED with a blending of commercial green (Ba$_2$SiO$_4$:Eu^{2+}) and red (CaAlSiN$_3$:Eu^{2+}) phosphors gives a high CRI (Ra = 83) demonstrating potential for near-UV white LEDs. The concept of exploiting inequivalent substitution of activator in mixed cation host is expected to open the gateway for developing phosphors with thermally stable luminescence.

ASSOCIATED CONTENT

Supporting Information

Calculation details and results for defect formation energies, supporting tables and figures, and crystal structure of K$_2$BaCa(PO$_4$)$_2$ (CIF). This material is available free of charge via the Internet at http://pubs.acs.org.

AUTHOR INFORMATION

Corresponding Author

* ninglx@mail.ahnu.edu.cn (L. Ning)

* xiazg@ustb.edu.cn (Z. Xia)

REFERENCES

(1) Pust, P.; Schmidt, P. J.; Schnick, W. A revolution in lighting. *Nat. Mater.* **2015**, 14, 454-458.

(2) Pust, P.; Weiler, V.; Hecht, C.; Tucks, A.; Wochnik, A. S.; Henss, A. K.; Wiechert, D.; Scheu, C.; Schmidt, P. J.; Schnick, W. Narrow-band red-emitting Sr[LiAl$_3$N$_4$]:Eu^{2+} as a next-generation LED-phosphor material. *Nat. Mater.* **2014**, 13, 891-896.

(3) Reineke, S. Complementary LED technologies. *Nat. Mater.* **2015**, 14, 459-462.

(4) Xia, Z. G.; Liu, Q. L. Progress in discovery and structural design of color conversion phosphors for LEDs. *Prog. Mater. Sci.* **2016**, 84, 59-117.

(5) Li, G. G.; Lin, C. C.; Chen, W.-T.; Molokeev, M. S.; Atuchin, V. V.; Chiang, C.-Y.; Zhou, W.; Wang, C.-W.; Li, W.-H.; Sheu, H.-S.; Chan, T.-S.; Ma, C. G.; Liu, R.-S. Photoluminescence Tuning via Cation Substitution in Oxonitridosilicate Phosphors: DFT Calculations, Different Site Occupations, and Luminescence Mechanisms. *Chem. Mater.* **2014,** 26, 2991-3001.

(6) Wei, Y.; Cao, L.; Lv, L. M.; Li, G. G.; Hao, J. R.; Gao, J. S.; Su, C. C.; Lin, C. C.; Jang, H. S.; Dang, P. P.; Lin, J. Highly Efficient Blue Emission and Superior Thermal Stability of BaAl$_{12}$O$_{19}$:Eu^{2+} Phosphors Based on Highly Symmetric Crystal Structure. *Chem. Mater.* **2018**, 30, 2389-2399.

(7) Xia, Z. G.; Liu, R.-S. Tunable Blue-Green Color Emission and Energy Transfer of Ca$_2$Al$_3$O$_6$F:Ce^{3+},Tb^{3+} Phosphors for Near-UV White LEDs. *J. Phys. Chem. C* **2012**, 116, 15604-15609.

(8) Daicho, H.; Iwasaki, T.; Enomoto, K.; Sasaki, Y.; Maeno, Y.; Shinomiya, Y.; Aoyagi, S.; Nishibori, E.; Sakata, M.; Sawa, H.; Matsuishi, S.; Hosono, H. A novel phosphor for glareless white light-emitting diodes. *Nat. Commun.* **2012**, 3, 1132.

(9) Lin, C. C.; Liu, R. S. Advances in Phosphors for Light-emitting Diodes. *J. Phys. Chem. Lett.* **2011**, 2, 1268-1277.

(10) Zhu, H.; Lin, C. C.; Luo, W.; Shu, S.; Liu, Z.; Liu, Y.; Kong, J.; Ma, E.; Cao, Y.; Liu, R. S.; Chen, X. Highly efficient non-rare-earth red emitting phosphor for warm white light-emitting diodes. *Nat. Commun.* **2014**, 5, 4312.

(11) Hermus, M.; Phan, P.-C.; Duke, A. C.; Brgoch, J. Tunable Optical Properties and Increased Thermal Quenching in the Blue-Emitting Phosphor Series: Ba$_2$(Y$_{1-x}$Lu$_x$)$_5$B$_5$O$_{17}$:Ce^{3+} (x = 0–1). *Chem. Mater.* **2017**, 29, 5267-5275.

(12) Im, W. B.; Brinkley, S.; Hu, J.; Mikhailovsky, A.; DenBaars, S. P.; Seshadri, R. Sr$_{2.975-x}$Ba$_x$Ce$_{0.025}$AlO$_4$F: a Highly Efficient Green-pEmitting Oxyfluoride Phosphor for Solid State White Lighting. *Chem. Mater.* **2010**, 22, 2842-2849.

(13) Im, W. B.; George, N.; Kurzman, J.; Brinkley, S.; Mikhailovsky, A.; Hu, J.; Chmelka, B. F.; DenBaars, S. P.; Seshadri, R. Efficient and color-tunable oxyfluoride solid

solution phosphors for solid-state white lighting. *Adv. Mater.* **2011,** 23, 2300-2305.

(14) Fan, X. T.; Chen, W. B.; Xin, S. Y.; Liu, Z. C.; Zhou, M.; Yu, X.; Zhou, D. C.; Xu, X. H.; Qiu, J. B. Achieving long-term zero-thermal-quenching with the assistance of carriers from deep traps. *J. Mater. Chem. C* **2018,** 6, 2978-2982.

(15) Zhang, X.; Wang, J.; Huang, L.; Pan, F.; Chen, Y.; Lei, B.; Peng, M.; Wu, M. Tunable Luminescent Properties and Concentration-Dependent, Site-Preferable Distribution of Eu^{2+} Ions in Silicate Glass for White LEDs Applications. *ACS Appl. Mater. Interfaces* **2015,** 7, 10044-10054.

(16) Lee, H. S.; Yoo, J. W. Yellow phosphors coated with TiO_2 for the enhancement of photoluminescence and thermal stability. *Appl. Surf. Sci.* **2011,** 257, 8355-8359.

(17) Zhuang, J. Q.; Xia, Z. G.; Liu, H. K.; Zhang, Z. P.; Liao, L. B. The improvement of moisture resistance and thermal stability of $Ca_3SiO_4Cl_2$:Eu^{2+} phosphor coated with SiO_2. *Appl. Surf. Sci.* **2011,** 257, 4350-4353.

(18) Kim, Y. H.; Arunkumar, P.; Kim, B. Y.; Unithrattil, S.; Kim, E.; Moon, S. H.; Hyun, J. Y.; Kim, K. H.; Lee, D.; Lee, J. S.; Im, W. B. A zero-thermal-quenching phosphor. *Nat. Mater.* **2017,** 16, 543-550.

(19) Chen, M. Y.; Xia, Z. G.; Molokeev, M. S.; Wang, T.; Liu, Q. L. Tuning of Photoluminescence and Local Structures of Substituted Cations in $xSr_2Ca(PO_4)_2$–$(1 - x)Ca_{10}Li(PO_4)_7$:Eu^{2+} Phosphors. *Chem. Mater.* **2017,** 29, 1430-1438.

(20) Xia, Z.; Liu, G.; Wen, J.; Mei, Z.; Balasubramanian, M.; Molokeev, M. S.; Peng, L.; Gu, L.; Miller, D. J.; Liu, Q.; Poeppelmeier, K. R. Tuning of Photoluminescence by Cation Nanosegregation in the $(CaMg)_x(NaSc)_{1-x}Si_2O_6$ Solid Solution. *J. Am. Chem. Soc.* **2016,** 138, 1158-1161.

(21) Xia, Z. G.; Xu, Z. H.; Chen, M. Y.; Liu, Q. L. Recent developments in the new inorganic solid-state LED phosphors. *Dalton Trans.* **2016,** 45, 11214-11232.

(22) Zhang, S.; Nakai, Y.; Tsuboi, T.; Huang, Y.; Seo, H. J. The thermal stabilities of luminescence and microstructures of Eu^{2+}-doped $KBaPO_4$ and $NaSrPO_4$ with beta-K_2SO_4 type structure. *Inorg. Chem.* **2011,** 50, 2897-2904.

(23) Song, H. J.; Yim, D. K.; Roh, H.-S.; Cho, I. S.; Kim, S.-J.; Jin, Y.-H.; Shim, H.-W.; Kim, D.-W.; Hong, K. S. $RbBaPO_4$:Eu^{2+}: a new alternative blue-emitting phosphor for UV-based white light-emitting diodes. *J. Mater. Chem. C* **2013,** 1, 500-505.

(24) Lin, C. C.; Xiao, Z. R.; Guo, G.-Y.; Chan, T.-S.; Liu, R.-S. Versatile phosphate phosphors $ABPO_4$ in white light-emitting diodes: collocated characteristic analysis and theoretical calculations. *J. Am. Chem. Soc.* **2010,** 132, 3020-3028.

(25) TOPAS, V. 2: General profile and structure analysis software for powder diffraction data–User's Manual; Bruker AXS: Karlsruhe, Germany. **2008.**

(26) Dudarev, S.; Botton, G.; Savrasov, S.; Humphreys, C.; Sutton, A. Electron-energy-loss spectra and the structural stability of nickel oxide: An LSDA+ U study. *Phys. Rev. B* **1998,** 57, 1505.

(27) Chaudhry, A.; Boutchko, R.; Chourou, S.; Zhang, G.; Grønbech-Jensen, N.; Canning, A. First-principles study of luminescence in Eu^{2+}-doped inorganic scintillators. *Phys. Rev. B* **2014,** 89.

(28) Kresse, G.; Furthmüller, J. Efficient iterative schemes for ab initio total-energy calculations using a plane-wave basis set. *Phys. Rev. B* **1996,** 54, 11169.

(29) Kresse, G.; Joubert, D. From ultrasoft pseudopotentials to the projector augmented-wave method. *Phys. Rev. B* **1999,** 59, 1758.

(30) Blöchl, P. E. Projector augmented-wave method. *Phys. Rev. B* **1994,** 50, 17953.

(31) Perdew, J. P.; Ernzerhof, M.; Burke, K. Rationale for mixing exact exchange with density functional approximations. *J. Chem. Phys.* **1996,** 105, 9982-9985.

(32) Freysoldt, C.; Grabowski, B.; Hickel, T.; Neugebauer, J.; Kresse, G.; Janotti, A.; Van de Walle, C. G. First-principles calculations for point defects in solids. *Rev. Mod. Phys.* **2014,** 86, 253.

(33) Launay, S.; Mahe, P.; Quarton, M. Polymorphisme et structure cristalline du monophosphate de sodium et baryum. *Mater. Res. Bull.* **1992,** 27, 1347-1353.

(34) Grau-Crespo, R.; Hamad, S.; Catlow, C. R. A.; Leeuw, N. H. d. Symmetry-adapted configurational modelling of fractional site occupancy in solids. *J. Phys-Condense. Mat.* **2007,** 19, 256201.

(35) Bhushan, S.; Chukichev, M. Temperature dependent studies of cathodoluminescence of green band of ZnO crystals. *J. Mater. Sci. Lett.* **1988,** 7, 319-321.

(36) Van den Eeckhout, K.; Smet, P. F.; Poelman, D. Persistent Luminescence in Eu^{2+}-Doped Compounds: A Review. *Materials* **2010,** 3, 2536-2566.

(37) Ning, L.; Cheng, W.; Zhou, C.; Duan, C.; Zhang, Y. Energetic, Optical, and Electronic Properties of Intrinsic Electron-Trapping Defects in $YAlO_3$: A Hybrid DFT Study. *J. Phys. Chem. C* **2014,** 118, 19940-19947.

(38) Chen, M. Y.; Xia, Z. G.; Molokeev, M. S.; Lin, C. C.; Su, C. C.; Chuang, Y.-C.; Liu, Q. L. Probing Eu^{2+} Luminescence from Different Crystallographic Sites in $Ca_{10}M(PO_4)_7$:Eu^{2+} (M = Li, Na, and K) with β-$Ca_3(PO_4)_2$-Type Structure. *Chem. Mater.* **2017,** 29, 7563-7570.